

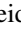






日本原子力研究開発機構機関リポジトリ  
Japan Atomic Energy Agency Institutional Repository

|              |  |
|--------------|--|
| Title        | Lifetime measurements of excited states in $^{55}\text{Cr}$  |
| Author(s)    | Kleis H., Seidlitz M, Blazhev A, Kaya L, Reiter P, Arnswald K., Dewald A, Droste M, Fransen C, Möller O, Shimizu Noritaka, Tsunoda Yusuke, Utsuno Yutaka, Von Brentano P, Zell K. O. |
| Citation     | Physical Review C,104(3),p.034310_1-034310_9   |
| Text Version | Published Journal Article  |
| URL          | <a href="https://jopss.jaea.go.jp/search/servlet/search?5072622">https://jopss.jaea.go.jp/search/servlet/search?5072622</a>  |
| DOI          | <a href="https://doi.org/10.1103/PhysRevC.104.034310">https://doi.org/10.1103/PhysRevC.104.034310</a>  |
| Right        | ©2021 American Physical Society  |

Lifetime measurements of excited states in  $^{55}\text{Cr}$ 

H. Kleis <sup>1</sup>, M. Seidlitz,<sup>1</sup> A. Blazhev,<sup>1</sup> L. Kaya,<sup>1</sup> P. Reiter <sup>1,\*</sup>, K. Arnswald <sup>1</sup>, A. Dewald,<sup>1</sup> M. Droste <sup>1</sup>, C. Fransen,<sup>1</sup> O. Möller,<sup>1,2</sup> N. Shimizu,<sup>3</sup> Y. Tsunoda <sup>3</sup>, Y. Utsuno,<sup>3,4</sup> P. von Brentano,<sup>1,†</sup> and K. O. Zell<sup>1</sup>

<sup>1</sup>*Institut für Kernphysik, Universität zu Köln, D-50937 Köln, Germany*

<sup>2</sup>*Institut für Kernphysik, Technische Universität Darmstadt, D-64289 Darmstadt, Germany*

<sup>3</sup>*Center for Nuclear Study, The University of Tokyo, Hongo, Bunkyo-ku, Tokyo 113-0033, Japan*

<sup>4</sup>*Advanced Science Research Center, Japan Atomic Energy Agency, Tokai, Ibaraki 319-1195, Japan*



(Received 17 May 2021; accepted 9 August 2021; published 10 September 2021)

Excited states in  $^{55}\text{Cr}$  have been populated via the fusion-evaporation reaction  $^{48}\text{Ca}(^{11}\text{B}, p3n)^{55}\text{Cr}$  at a beam energy of 32 MeV. The Cologne plunger device surrounded by a  $\gamma$ -ray detector array was employed to determine lifetimes with the recoil-distance Doppler-shift method.  $\gamma$  rays were observed by one Ge EUROBALL cluster detector and five HPGe detectors.  $\gamma\gamma$ -coincidence data were analyzed with help from the differential decay-curve method, and precise lifetimes for the first excited states were extracted from the  $5/2^- \rightarrow 3/2^-$  and the  $9/2^- \rightarrow 5/2^-$  transitions. Reduced transition strengths  $B(\sigma\lambda)$  were determined and compared to shell-model calculations employing four interactions KB3G, FPD6, GXPF1A, and GXPF1Br. The calculations were also performed for the  $N = 31$  isotonic chain from  $^{53}\text{Ti}$  to  $^{61}\text{Zn}$ . Inspection of the wave functions as well as particle-plus-rotor model calculations allow for a detailed understanding of the excited states and the reduced transition strength in  $^{55}\text{Cr}$ . The interactions GXPF1A and GXPF1Br reproduce well the experimental findings in  $^{55}\text{Cr}$  and in other isotones.

DOI: [10.1103/PhysRevC.104.034310](https://doi.org/10.1103/PhysRevC.104.034310)

## I. INTRODUCTION

The shell structure of neutron-rich nuclei between the  $N = 20$  and the 28 isotonic sequences was first explained in terms of the monopole part of the nucleon-nucleon residual interaction [1–3]. The missing protons at large neutron excess cause monopole shifts of neutron single-particle orbits and, thus, generate new shell gaps [4,5]. The details of the proton-neutron coupling within a major shell and the shell evolution in neutron-rich Ca and Ni nuclei was studied with modern effective interactions. The neutron orbits  $1f_{5/2}$ ,  $2p_{3/2}$ , and  $2p_{1/2}$  are the subjects of the tensor- and central-force monopole contributions. It was found that both forces contribute additively to a sharp rise of the  $1f_{5/2}$  orbit relative to the  $2p_{3/2}$  and  $2p_{1/2}$  orbits by removing protons along neutron-rich isotones  $N \geq 28$  from  $^{56}\text{Ni}$  to  $^{48}\text{Ca}$  [6]. The GXPF1Br interaction is introduced to describe a neutron-neutron interaction which is necessary to describe the shell evolution from  $^{48}\text{Ca}$  to  $^{54}\text{Ca}$  with two pronounced shell gaps at  $N = 32$  and at  $N = 34$  [7].

For the neutron-rich chromium nuclei halfway between the Ca and the Ni isotopes, the following shell-model characteristics can be expected. Above the doubly magic  $^{48}\text{Ca}$ , subshell closures occur between the neutron  $\nu p_{3/2}$  and  $\nu p_{1/2}$  and between the  $\nu p_{1/2}$  and  $\nu f_{5/2}$  orbits. The shell evolution of neutron orbits along neutron-rich isotones  $N \geq 30$  from Ca to Ni is subject to the attractive interaction between the

$1f_{7/2}$  proton and the  $1f_{5/2}$  neutron orbits due to the tensor and central forces. Additional protons lower the energy of the neutron  $1f_{5/2}$  orbit. For  $^{55}\text{Cr}$  isotopes, the  $1f_{5/2}$  orbit is expected to be close to the  $2p_{3/2}$  orbit. The interplay of the  $1f_{5/2}$ ,  $2p_{3/2}$ , and  $2p_{1/2}$  orbits along the  $N = 31$  isotones from Ti to Zn is studied within this paper by comparing experimental excitation energies and transition probabilities of low-lying states with the results of shell-model calculations employing the FPD6, KB3G, GXPF1A, and GXPF1Br interactions.

Although shell evolution is one of the important ingredients to understand the structure of  $^{55}\text{Cr}$ , collectivity is another crucial factor. In the neutron-rich Cr and Fe regions, the appearance of the deformed region around  $N = 40$  is well known, which is analogous to the “island of inversion” around  $^{32}\text{Mg}$ . A detailed study of lighter  $N = 29$ – $35$  isotopes in Cr and Fe was performed in order to investigate natural- and unnatural-parity states as a function of angular momentum by means of large-scale shell-model calculations employing the model space of  $fp$ -shell +  $1g_{9/2}$  +  $2d_{5/2}$  orbits [8]. Among other results, these shell-model calculations describe and predict the energy levels of both natural- and unnatural-parity states up to the high-spin states in  $^{55}\text{Cr}$ . The calculations yield total-energy surfaces for the negative- and positive-parity states in odd-mass  $^{55-59}\text{Cr}$  and  $^{57-61}\text{Fe}$  indicating the dominance of prolate deformation.

The excited states on top of the deformed ground states are grouped in rotational bands according to the particle-plus-rotor model. In order to establish a comprehensive picture of this region, it is important to simultaneously understand shell evolution and collectivity. Lifetime measurements provide crucial information on the character of the excited states.

\*Corresponding author: preiter@ikp.uni-koeln.de

†Deceased.

The most recent and comprehensive study of  $^{55}\text{Cr}$  was previously performed by Ref. [9] covering excitation energies above 12 MeV and positive-parity state spins up to  $33/2^+$ . The level scheme was compared with the results of shell-model calculations using the effective interactions GXPF1A, GXPF1B, and KB3G. The GXPF1A and GXPF1B interactions provide a general agreement with the negative-parity states in  $^{55}\text{Cr}$ . The negative-parity band structures in  $^{55}\text{Cr}$  are related to two different configurations: a  $f_{5/2}$  neutron outside the  $^{54}\text{Cr}$  core and  $p_{3/2}$  neutron-hole states relative to  $N = 32$ .

In neighboring nuclei  $^{54,56}\text{Cr}$  the first excited  $2^+$  states were populated by Coulomb excitation at relativistic energies, and  $\gamma$  rays were measured using the RISING setup at GSI [10]. For  $^{56}\text{Cr}$  the  $B(E2, 2^+ \rightarrow 0^+)$  values were determined as 8.7(3.0) W.u. (where W.u. represents the Weisskopf unit). A more precise measurement for the first  $2^+$  and  $4^+$  states in  $^{56}\text{Cr}$  yielded lifetime value of  $\tau = 5.49 \pm 0.14$  ps for the first  $2^+$  state corresponding to an improved  $B(E2, 2^+ \rightarrow 0^+)$  value of 11.3(3) W.u. For the  $4^+ \rightarrow 2^+$  transition the lifetime value of  $\tau = 3.15 \pm 0.11$  ps corresponds to a  $B(E2, 4^+ \rightarrow 2^+)$  value of 14.6(5) W.u. [11]. The  $B(E2, 2^+ \rightarrow 0^+)$  value of  $^{56}\text{Cr}$  is smaller than those of  $^{54,58}\text{Cr}$  corroborating a sub-shell closure at neutron number  $N = 32$  which was already anticipated by the higher energy of the  $2_1^+$  state in  $^{56}\text{Cr}$  [11].

The paper is organized as follows: The experimental setup and its details are the subject of Sec. II. The data analysis of the experiment and the lifetime results for the first  $9/2^-$  and  $5/2^-$  states are described in Sec. III. A comparison between experimental findings and shell-model calculations, that are based on four different interactions KB3G, FPD6, GXPF1A, and GXPF1Br is given in Sec. IV. The paper closes with a summary and conclusions in Sec. V.

## II. EXPERIMENTAL DETAILS

Excited states in  $^{55}\text{Cr}$  were populated by the fusion-evaporation reaction  $^{48}\text{Ca}(^{11}\text{B}, p3n)^{55}\text{Cr}$  with a relative cross section of 0.5%. The  $^{11}\text{B}$  beam was accelerated to 32 MeV by the FN tandem accelerator at the University of Cologne. The target consisted of a 0.5-mg/cm<sup>2</sup>-thick layer of enriched  $^{48}\text{Ca}$  that had been evaporated onto a 2.0-mg/cm<sup>2</sup>-thick gold foil facing the beam. An additional gold layer with a thickness of 40  $\mu\text{g}/\text{cm}^2$  protected the  $^{48}\text{Ca}$  layer from oxidation. The recoiling  $^{55}\text{Cr}$  nuclei left the target with a velocity of approximately 1% of the speed of light and were stopped in a  $^{197}\text{Au}$  stopper foil with a thickness of 2.2 mg/cm<sup>2</sup>. To determine the lifetimes of excited states in  $^{55}\text{Cr}$  12 individual measurements were performed, each at a different target-to-stopper distance in the range between 0.5 and 80  $\mu\text{m}$ . The distance between the target and the stopper foil was precisely monitored and controlled during the experiment by a capacitive feedback system employing a piezoelectric linear motor in order to compensate beam-dependent changes as, e.g., thermal expansion [13].

A setup of one EUROBALL cluster detector, containing seven HPGe crystals and five single HPGe detectors were employed to detect the emitted  $\gamma$  rays. The EUROBALL detector was placed at a distance of 8.5 cm between the target and the front side of the central HPGe detector. Thus, the

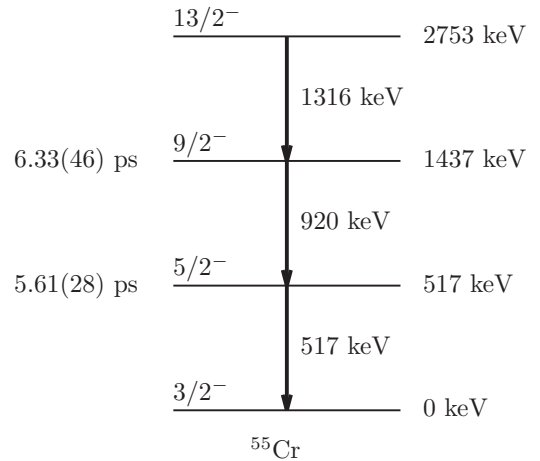


FIG. 1. Partial level scheme of populated excited states and measured lifetimes in  $^{55}\text{Cr}$ . The indicated spins, level, and transition energies are from Refs. [9,12].

seven crystals in the EUROBALL cluster were positioned in a ring of six HPGe detectors at the same forward angle of  $27.4^\circ$  relative to the beam axis and one detector at  $0^\circ$ . The other five single HPGe detectors were arranged in a ring at polar angles of  $143^\circ$ . Additional information of the setup is given in Ref. [11]. The experiment was based on the recoil-distance Doppler-shift method combined with the differential decay-curve method in order to determine nuclear-level lifetimes in the picosecond range [13,14]. Two-dimensional  $\gamma\gamma$ -coincidence matrices were sorted and analyzed for each individual target-to-stopper distance and for the different combinations of detector rings. In total  $8.1 \times 10^9$   $\gamma\gamma$  events were recorded. Utilizing  $\gamma$ -gated spectra, any uncertainties by unknown side feeding were eliminated.

## III. DATA ANALYSIS AND RESULTS

The partial level scheme of  $^{55}\text{Cr}$  including spins, level, and transition energies as well as the experimentally deduced level lifetimes is given in Fig. 1. The coincidence spectra of the  $5/2^- \rightarrow 3/2^-$   $\gamma$ -ray transition are shown in Figs. 2(a)–2(c), and corresponding spectra for the  $9/2^- \rightarrow 5/2^-$  transition are depicted in Figs. 2(d)–2(f). The intensity distribution of the  $5/2^- \rightarrow 3/2^-$  transition at 517 keV was analyzed after gating on the Doppler-shifted component of the directly feeding  $9/2^- \rightarrow 5/2^-$  transition at 920 keV for all target-to-stopper distances. The evolution of the line shape of the  $9/2^- \rightarrow 5/2^-$  transition was analyzed accordingly by a gate on the Doppler-shifted component of the feeding  $13/2^- \rightarrow 9/2^-$  transition with a transition energy of 1316 keV. Details on the analysis procedure are described in Refs. [13,14]. The changing intensity distributions of the Doppler-shifted and unshifted components for different distances can be observed unambiguously. The recoil velocity was determined from experiment via the observed Doppler shift of the  $\gamma$  ray transition of  $^{55}\text{Cr}$  at given detection angles and yielded  $\beta = 1\%$  of speed of light. The low momentum transfer of the reaction and considerable energy straggling in the target resulted in a broad

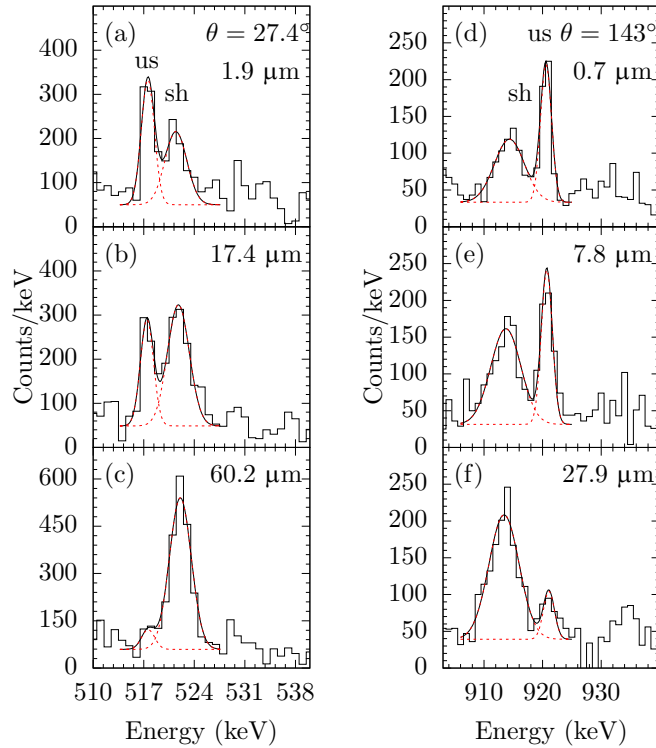


FIG. 2. The  $\gamma$ -ray energy spectra for three different target-to-stopper distances are shown for (a)–(c) the  $5/2^- \rightarrow 3/2^-$  transition at 517 keV and for (d) and (e) the  $9/2^- \rightarrow 5/2^-$  transition at 920 keV. Spectra are produced by a gate on the Doppler-shifted part of the directly feeding transitions at 920 and 1316 keV, respectively. Unshifted (us) and shifted (sh) components are labeled. The final fitted Gaussian curves for the unshifted and shifted components and a background contribution are shown (see the text for details).

velocity distribution of the recoiling nuclei after the target, i.e., a wide range of flight times between target and stopper foil. Thus, the observed velocity distribution of the nuclei that emit a  $\gamma$  ray in flight, depended on the target-to-stopper distance. A correction was applied which normalized the distances to the observed maximum recoil velocities (cf. Refs. [15,16]).

For each target-to-stopper distance  $i$  in the sensitive range an individual statistically independent lifetime  $\tau_i = I_{us}(t)/\frac{d}{dt}I_{sh}(t)$ , where  $I_{sh,us}(t)$  are the measured intensities of the Doppler-shifted and unshifted components, respectively, was calculated using the program NAPATAU [17]. Example spectra are shown in Fig. 3. For each combination of detector rings a mean lifetime value  $\bar{\tau}$  was calculated using the weighted mean of the different lifetimes  $\tau_i$  [13]. The final lifetime values  $\tau$  for the  $9/2^-$  and  $5/2^-$  states correspond to the weighted mean of the lifetime values from the different combinations of detector rings. Systematic uncertainties are mainly caused by the velocity distribution of the recoiling nuclei due to the opening angle of the detectors with  $\Delta\theta = 3^\circ$ . Systematic errors due to the feedback system of the plunger and the thickness of the target are negligible with respect to the angle uncertainty. Due to small gates further systematic uncertainties from unknown contaminants in the same energy region of the transitions of interest are also marginal.

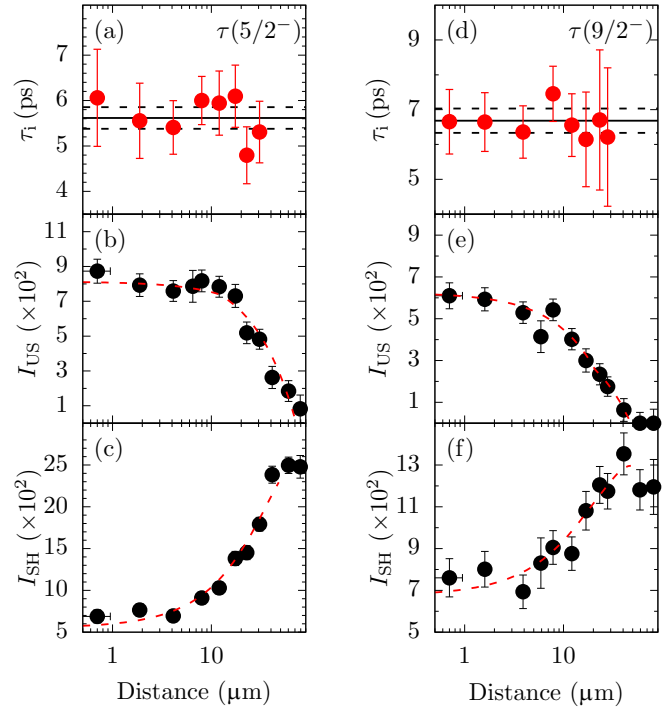


FIG. 3. Lifetime values  $\tau_i$  and  $\gamma$ -ray intensities are plotted against the relative target-to-stopper distances for one combination of detector rings for the (a)–(c)  $5/2^-$  state and (d)–(f) the  $9/2^-$  state. The weighted mean lifetime value of the individual  $\tau_i$  is marked with a black solid line, and the black dashed line indicates the statistical uncertainty. The respective unshifted [(b) and (e)] and shifted [(c) and (f)] intensities are presented together with corresponding polynomial fit functions (dashed red curves). Note the logarithmic distance scale.

Doppler-shift attenuation effects of the slowing-down process of the nuclei in the stopper foil are negligible for lifetimes in the  $\tau \gtrsim 5$ -ps range.

The study of the  $5/2^- \rightarrow 3/2^-$  ground-state (g.s.) decay at 517 keV yields a new lifetime value of  $\tau = 5.61(28)$  ps for the  $5/2^-$  state. For this value the individually derived lifetimes from the statistically independent analyses of four different combinations of detector rings were included. Due to the  $E2/M1$  mixing of the 517-keV transition, reduced transition probabilities depend on the exact amount of the mixing. Evaluated data imply a dominant dipole character of the radiation. A measurement of  $\gamma\gamma$ -angular correlation for the determination of  $\delta$  was not feasible with the detector setup in this experiment.

However, angular distributions were measured in previous experiments by the multidetector spectrometers Yale Rochester Array for SpecTroscope ball [12] and Gammasphere [9]. In both experiments the multipolarity of the observed transitions was determined from the angular-distribution analysis via a fit with Legendre polynomials. The usual ratios of  $A_2/A_0$  and  $A_4/A_0$  values of the polynomial fit were used to determine the type of  $\gamma$ -ray transition, i.e., a stretched/unstretched, dipole/quadrupole transition. A pure dipole transition has a negative  $A_2/A_0$  coefficient, whereas a stretched quadrupole should have a positive  $A_2/A_0$  coefficient.

TABLE I. Experimentally deduced lifetime values compared with previously published lifetime values (from Ref. [18]) for  $^{55}\text{Cr}$ .

| $J_i^\pi \rightarrow J_f^\pi$ | $E_x$ (keV) | $\tau$ (ps) | $\tau_{\text{Lit.}}$ (ps) |
|-------------------------------|-------------|-------------|---------------------------|
| $5/2_1^- \rightarrow 3/2_1^-$ | 517         | 5.61(28)    | $< 7.5$                   |
| $9/2_1^- \rightarrow 5/2_1^-$ | 1437        | 6.33(46)    | 6(2)                      |

The results of Refs. [9,12] yielded negative values of  $A_2/A_0 = -0.23(1)$  and  $-0.35(3)$ , respectively, for the  $5/2^- \rightarrow 3/2^-$  transition. These  $A_2/A_0$  values correspond to a very small mixing ratio  $\delta = 0.080$  and  $\delta = 0.025$  for the other experiment assuming complete alignment. From the calculated  $B(M1)$  and  $B(E2)$  strengths of the GXPF1A interaction a theoretical mixing ratio is calculated  $\delta_{\text{theo}} = 0.024$  which is consistent with the experiment. Detailed explanations of the shell-model calculation are given in the following Sec. IV. The new lifetime value from this experiment corresponds to  $B(M1) = 41(2) \times 10^{-3}$  and  $B(E2) = 0.87_{-0.66}^{+1.24}$  W.u. The  $B(E2)$  value is calculated with the mean of the mixing ratios from the two previous experiments and the uncertainty with the range of these mixing ratios. The lifetime of the first  $9/2^-$  state with an excitation energy of 1437 keV was determined to  $\tau = 6.33(46)$  ps. For the evaluation of the lifetime three out of four combinations of detector rings were used due to low statistics in the  $p3n$  channel. The corresponding new  $B(E2) = 12.9(10)$  W.u. value from this experiment has a much reduced uncertainty and it agrees well with respect to the previous value of  $B(E2) = 13.6_{-3.4}^{+6.8}$  W.u. of Ref. [18]. The new lifetime results, obtained in the experiment, are summarized in Table I.

#### IV. SHELL-MODEL CALCULATIONS

In order to assess the relevance of the newly determined reduced transition probabilities shell-model calculations with different interactions were performed not only for  $^{55}\text{Cr}$ , but also along the chain of even-odd  $N = 31$  isotones for  $^{53}\text{Ti}$ ,  $^{55}\text{Cr}$ ,  $^{57}\text{Fe}$ ,  $^{59}\text{Ni}$ , and  $^{61}\text{Zn}$ , respectively. Moreover, a detailed analysis of the wave functions of the  $3/2_{\text{g.s.}}^-$ ,  $5/2^-$ ,  $9/2^-$  in  $^{55}\text{Cr}$  was performed.

For the theoretical description of the excitation energies and the  $B(E2)$  and  $B(M1)$  values of the ground-state band, shell-model calculations were performed employing the KSHELL code [19] as well as the code NUSHELLX@MSU [20]. The  $fp$  model space comprises the  $0f_{7/2}$ ,  $1p_{3/2}$ ,  $1p_{1/2}$ , and  $0f_{5/2}$  orbitals, coupled to a  $^{40}\text{Ca}$  core. Four interactions were employed for comparison with the present experimental data: FPD6 [21], KB3G [22], GXPF1A [23,24], and GXPF1Br [7]. The first three shell-model interactions are well established in the  $fp$  model space based on the fit of the experimental data especially the GXPF1A interaction is applied to reproduce and predict the properties of nuclei in the regions of  $Z$  or  $N$  from 20 to 40. The last one, the GXPF1Br interaction, is obtained by modifying the GXPF1B interaction in order to reproduce latest experimental data from very neutron-rich Ca isotopes, in particular, the new neutron magic numbers at  $N = 32$  and  $N = 34$ .

TABLE II. Experimentally deduced excitation energies (from Refs. [18,27–31]) compared with shell-model calculations for the even-odd  $N = 31$  isotones from  $^{53}\text{Ti}$  to  $^{61}\text{Zn}$ . Additional information is given in the text.

| $^A X$           | $J^\pi$ | $E_x$ (keV) |        |      |        |         |
|------------------|---------|-------------|--------|------|--------|---------|
|                  |         | Expt.       | Theory |      |        |         |
|                  |         |             | FPD6   | KB3G | GXPF1A | GXPF1Br |
| $^{53}\text{Ti}$ | $5/2^-$ | 1237        | 612    | 1137 | 1356   | 1391    |
|                  | $9/2^-$ | 2205        | 1735   | 2124 | 2230   | 2220    |
| $^{55}\text{Cr}$ | $5/2^-$ | 517         | 366    | 190  | 533    | 368     |
|                  | $9/2^-$ | 1437        | 1514   | 1132 | 1499   | 1333    |
| $^{57}\text{Fe}$ | $5/2^-$ | 136         | 308    | -182 | 76     | -51     |
|                  | $9/2^-$ | 1198        | 1610   | 1009 | 1139   | 1041    |
| $^{59}\text{Ni}$ | $5/2^-$ | 339         | 294    | 248  | 363    | 218     |
|                  | $9/2^-$ | 1767        | 2161   | 1492 | 1845   | 1698    |
| $^{61}\text{Zn}$ | $5/2^-$ | 124         | 234    | -386 | 106    | -123    |
|                  | $9/2^-$ | 1266        | 1744   | 1025 | 1290   | 1153    |

For all calculations the  $B(E2)$  values were computed with the effective charges  $e_\pi = 1.23e$  and  $e_\nu = 0.54e$  which are taken from Ref. [25] as in the original paper [24] and the free-nucleon  $g_s$  factors with a quenching of 0.9 following the least-squares fit of the  $pf$ -shell nuclei in Ref. [26] were used to calculate the  $B(M1)$  strengths. We use harmonic-oscillator radial wave functions with the parametrization  $\hbar\omega = 45A^{-1/3} - 25A^{-2/3}$  MeV. All calculated excitation energies for the first  $5/2^-$  state and  $9/2^-$  state and the experimentally determined excitation energies from previous experiments are given in Table II. In contrast to the other given isotones, the ground state of  $^{57}\text{Fe}$  is not a  $3/2^-$  state but a  $1/2^-$  state. Excitation energies are given in this case with respect to the  $1/2^-$  ground state. The first  $3/2^-$  state has an excitation energy of 14.4 keV. For  $^{57}\text{Fe}$  and  $^{61}\text{Zn}$  the interactions KB3G and GXPF1Br predict the  $5/2^-$  state as the ground state. In Table II and Fig. 4 negative values for the excitation energy are given for these nuclei because the  $5/2^-$  energy is calculated relative to the  $3/2^-$  energy.

The excitation energies of the excited  $5/2^-$  state relative to the  $3/2^-$  state and the  $B(M1; 5/2^- \rightarrow 3/2^-)$  values for all five  $N = 31$  isotones and all four shell-model interactions are presented in Figs. 4(a) and 4(b) (see Tables II and III). The GXPF1A interaction is in very good agreement with the experimental results for the excitation energies of the  $5/2^-$  state along the isotonic chain, which is also true for excitation energies of the  $9/2^-$  state [see Fig. 5(a)]. The GXPF1Br interaction underestimates the excitation energies of the  $5/2^-$  state with increasing proton number. However, GXPF1Br reproduces reasonably well the excitation energies of the  $9/2^-$  state [see Fig. 5(a)]. The calculated energies for the  $5/2^-$  state from the FPD6 interaction show a continuous decline in the energy values and do not reproduce the experimental values. Close to the shell closure at  $^{53}\text{Ti}$ , and for the direct neighbors of  $^{59}\text{Ni}$ ,  $^{57}\text{Fe}$ , and  $^{61}\text{Zn}$ , the theoretical values do not agree with experiment. The KB3G interaction show obvious deviation between calculated and experimental excitation energies for the  $5/2^-$  state of the isotones  $^{55}\text{Cr}$  and  $^{61}\text{Zn}$ .

TABLE III. Experimentally deduced transition probabilities for the isotones along  $N = 31$  (from Refs. [18,27–34] and for  $^{55}\text{Cr}$  from this paper) compared with shell-model calculations using charges  $e_\pi = 1.23e$  and  $e_\nu = 0.54e$  with quenching of 0.9 from the free nucleon  $g_s$  factors.

| ${}^A_Z X$       | $J_i^\pi \rightarrow J_f^\pi$ | $E_x$ (keV) | $\sigma\lambda$ | $B(\sigma\lambda) \downarrow$ (W.u.) |                        |                        |                        |                       |
|------------------|-------------------------------|-------------|-----------------|--------------------------------------|------------------------|------------------------|------------------------|-----------------------|
|                  |                               |             |                 | Experiment                           | Theory                 |                        |                        |                       |
|                  |                               |             |                 |                                      | FPD6                   | KB3G                   | GXPFI1A                | GXPFI1Br              |
| $^{53}\text{Ti}$ | $5/2_1^- \rightarrow 3/2_1^-$ | 1237        | $M1$            | $\leq 22.34 \times 10^{-3}$          | $9.29 \times 10^{-3}$  | $79.86 \times 10^{-3}$ | $94.13 \times 10^{-3}$ | $88.8 \times 10^{-3}$ |
|                  |                               |             |                 | $E2$                                 | $\leq 31.29$           | 0.047                  | 3.36                   | 6.93                  |
| $^{55}\text{Cr}$ | $9/2_1^- \rightarrow 5/2_1^-$ | 2205        | $E2$            | $2.7^{+1.1}_{-0.8}$                  | 5.98                   | 8.27                   | 7.17                   | 7.22                  |
|                  | $5/2_1^- \rightarrow 3/2_1^-$ | 517         | $M1$            | $41(2) \times 10^{-3}$               | $13.78 \times 10^{-3}$ | $21.88 \times 10^{-3}$ | $8.95 \times 10^{-3}$  | $8.55 \times 10^{-3}$ |
|                  |                               |             | $E2$            | $0.87^{+1.24}_{-0.66}$               | 1.695                  | 0.503                  | 0.035                  | 0.039                 |
| $^{57}\text{Fe}$ | $9/2_1^- \rightarrow 5/2_1^-$ | 1437        | $E2$            | $12.9(10)^a$                         | 15.64                  | 15.07                  | 15.49                  | 15.37                 |
|                  | $5/2_1^- \rightarrow 3/2_1^-$ | 136         | $M1$            | $1.18(17) \times 10^{-3}$            | $12.02 \times 10^{-3}$ | $1.40 \times 10^{-3}$  | $0.002 \times 10^{-3}$ | $0.22 \times 10^{-3}$ |
|                  |                               |             | $E2$            | 2.3(4)                               | 0.061                  | 0.209                  | 2.71                   | 2.38                  |
| $^{59}\text{Ni}$ | $9/2_1^- \rightarrow 5/2_1^-$ | 1198        | $E2$            | 11.1(16)                             | 15.73                  | 15.16                  | 16.38                  | 16.33                 |
|                  | $5/2_1^- \rightarrow 3/2_1^-$ | 339         | $M1$            | $8.1(10) \times 10^{-3}$             | $8.11 \times 10^{-3}$  | $3.07 \times 10^{-3}$  | $4.61 \times 10^{-3}$  | $5.75 \times 10^{-3}$ |
|                  |                               |             | $E2$            | 0                                    | 1.444                  | 0.0198                 | 0.238                  | 0.34                  |
| $^{61}\text{Zn}$ | $9/2_1^- \rightarrow 5/2_1^-$ | 1767        | $E2$            | 10(3)                                | 2.46                   | 2.57                   | 3.51                   | 3.50                  |
|                  | $5/2_1^- \rightarrow 3/2_1^-$ | 124         | $M1$            | $3.5(8) \times 10^{-3}$              | $6.11 \times 10^{-3}$  | $3.16 \times 10^{-3}$  | $3.40 \times 10^{-3}$  | $3.74 \times 10^{-3}$ |
|                  |                               |             | $E2$            | $1.0^{+10}_{-6}$                     | 3.56                   | 0.42                   | 0.17                   | 0.1                   |
|                  | $9/2_1^- \rightarrow 5/2_1^-$ | 1266        | $E2$            | $21.66^{+2.66}_{-2.24}$              | 15.41                  | 15.16                  | 15.84                  | 15.64                 |

<sup>a</sup>Value is deduced from the branching ratio of 0.201(9) (from Ref. [9]) for this transition.

The highest  $B(M1; 5/2^- \rightarrow 3/2^-)$  value of  $41(2) \times 10^{-3}$  W.u. was found for  $^{55}\text{Cr}$  [see Fig. 4(b)]. In neighboring isotones only an upper limit was recently published for  $^{53}\text{Ti}$  by Ref. [32] and a low value of  $1.18(17) \times 10^{-3}$  W.u. is known for  $^{57}\text{Fe}$ . At the shell closure the  $B(M1; 5/2^- \rightarrow 3/2^-)$  transition strength increases to  $8.1(10) \times 10^{-3}$  W.u., and it is lower again for  $^{61}\text{Zn}$ . The comparison between experiment and theory demonstrates that none of the interactions and their theoretical  $B(M1; 5/2^- \rightarrow 3/2^-)$  values do reproduce the measured pattern. Although the outcome of the comparison with respect to the excitation energies was best for the GXPFI1A interaction, clear discrepancies occur at lower proton numbers for the  $B(M1; 5/2^- \rightarrow 3/2^-)$  value of  $^{53}\text{Ti}$  and  $^{55}\text{Cr}$  for GXPFI1A. A very similar behavior is observed for the KB3G interaction and the  $B(M1; 5/2^- \rightarrow 3/2^-)$  values. At  $^{57}\text{Fe}$ ,  $^{59}\text{Ni}$  the experimental trend is reproduced by GXPFI1A and KB3G, and for  $^{61}\text{Zn}$  the measured  $B(M1; 5/2^- \rightarrow 3/2^-)$  value is very well reproduced by the two interactions GXPFI1A and KB3G.

The FPD6 interaction does reasonably well reproduce the experimental  $B(M1; 5/2^- \rightarrow 3/2^-)$  values for four isotones  $^{53}\text{Ti}$ ,  $^{55}\text{Cr}$ ,  $^{59}\text{Ni}$ , and  $^{61}\text{Zn}$ . However, at  $Z = 26$  the  $^{57}\text{Fe}$  value does neither concur with the experimental value nor with the results obtained with GXPFI1A and KB3G. It disagrees with the results from the other two interactions by nearly one order of magnitude. To summarize, the newly measured  $B(M1; 5/2^- \rightarrow 3/2^-)$  value in  $^{55}\text{Cr}$  is underestimated by all shell-model interactions by a factor of 2 and more.

In Fig. 5 the excitation energies from the excited  $9/2^-$  state and the  $B(E2; 9/2^- \rightarrow 5/2^-)$  values for the  $N = 31$  isotones  $^{53}\text{Ti}$ ,  $^{55}\text{Cr}$ ,  $^{57}\text{Fe}$ ,  $^{59}\text{Ni}$ , and  $^{61}\text{Zn}$  for all four interactions are shown. The theoretical excitation energies of all the excited

$9/2^-$  state are best reproduced by the GXPFI1A interaction. The GXPFI1Br results also reproduce the general behavior along the chain of isotones. For the four nuclei heavier than  $^{53}\text{Ti}$ , the theoretical energy values are, in average, 110 keV below the experimental ones. In general, the FPD6 and KB3G results show a larger discrepancy between experiment and theory, whereas KB3G energy values clearly underestimate all five experimental values, the FPD6 energies are clearly below the experimental results for  $^{53}\text{Ti}$  and above the experimental results for  $^{55}\text{Cr}$ ,  $^{57}\text{Fe}$ ,  $^{59}\text{Ni}$ , and  $^{61}\text{Zn}$ .

The theoretical  $B(E2; 9/2^- \rightarrow 5/2^-)$  values show all comparable results for the five isotones and the four interactions, respectively. Detailed comparison between theoretical and experimental  $B(E2; 9/2^- \rightarrow 5/2^-)$  values yield that the experimental  $B(E2)$  values are overestimated for the first three nuclei  $^{53}\text{Ti}$ ,  $^{55}\text{Cr}$ , and  $^{57}\text{Fe}$  and underestimated for  $^{59}\text{Ni}$  and  $^{61}\text{Zn}$ . All interactions show the lowest  $B(E2; 9/2^- \rightarrow 5/2^-)$  values at  $Z = 28$  ( $^{59}\text{Ni}$ ) which may be attributed to the closed proton shell. In contrast to theory, the experimental values and the experimental trend in the isotones indicate a smooth and open core at  $^{59}\text{Ni}$ .

Compared with the isotopes  $^{54,56}\text{Cr}$  where the experimental lifetime values for the  $2^+$  state correspond to  $B(E2; 2^+ \rightarrow 0^+_{\text{g.s.}}) = 14.6(6)$  and  $11.33(31)$  W.u. the experimental  $B(E2; 9/2^- \rightarrow 5/2^-) = 12.9(10)$  W.u. in  $^{55}\text{Cr}$  is between the two values and corroborates the previous finding of a subshell closure at  $N = 32$  [11].

The new  $B(M1; 5/2^- \rightarrow 3/2^-)$  and  $B(E2; 9/2^- \rightarrow 5/2^-)$  values allow us to elucidate in detail the shell-model results, especially the various configurations of the individual states. We have analyzed the wave function of  $^{55}\text{Cr}$  for three shell-model interactions FPD6, KB3G, and GXPFI1A for the

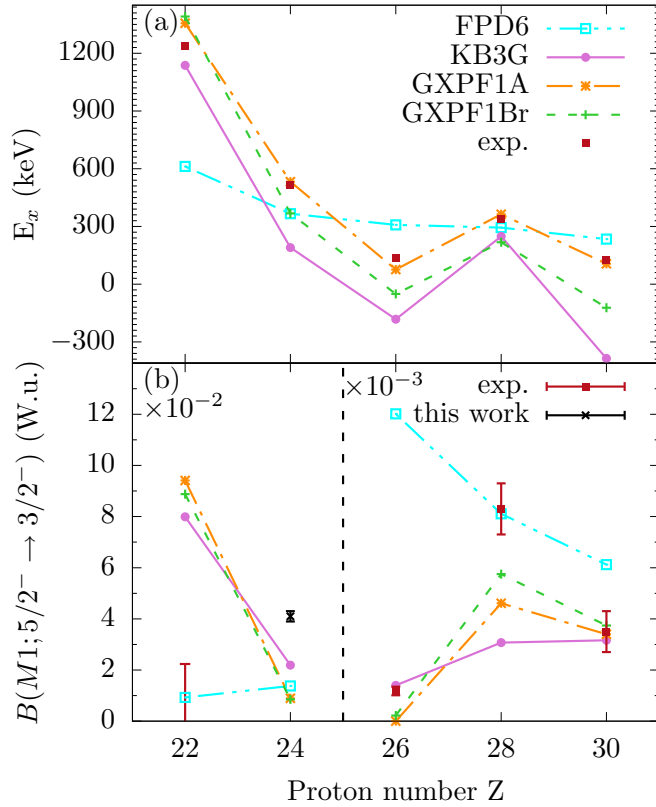


FIG. 4. (a) Calculated and experimental excitation energies  $E_x$  in keV for the  $5/2^-$  state and (b)  $B(M1, 5/2^- \rightarrow 3/2^-)$  values in W.u. (from Refs. [18,27–32] and this paper) for the isotones  $^{53}\text{Ti}$ ,  $^{55}\text{Cr}$ ,  $^{57}\text{Fe}$ ,  $^{59}\text{Ni}$ , and  $^{61}\text{Zn}$  with  $N = 31$ . The shell-model interactions FPD6, KB3G, GXPF1A, and GXPF1Br are employed for the calculation. (Please note the change in scale between  $Z = 24$  and  $Z = 26$ .)

$3/2^-$  ground state and the  $5/2_1^-$  and  $9/2_1^-$  states. The dominant wave function contributions are presented in Fig. 6. For all configurations shown the four valence protons occupy the  $\pi(f_{7/2})^4$  configuration and eight out of the eleven valence neutrons reside in the  $\nu(f_{7/2})^8$  configuration. For the  $3/2^-$  ground state the FPD6 interaction yields the neutron  $\nu(f_{7/2})^8(p_{3/2})^1(f_{5/2})^2$  contribution to be the dominant part of the wave function, whereas the KB3G and GXPF1A interactions describe the  $3/2^-$  ground state to be mainly a  $\nu(f_{7/2})^8(p_{3/2})^3$  configuration. For the excited  $5/2^-$  and  $9/2^-$  states the dominant configuration of the wave function is the  $\nu(f_{7/2})^8(p_{3/2})^2(f_{5/2})^1$  part for all interactions.

The wave function contents can explain the difference in the calculated  $B(M1)$  value between the FPD6 interaction and the other interactions. In case of the FPD6 interaction, the dominant part of the transitions is given by the  $\nu f_{5/2} \leftrightarrow \nu p_{3/2}$  transition, and this corresponds to a weak  $B(M1)$  value which is not observed in experiment. The spin-flip transition  $\nu p_{1/2} \leftrightarrow \nu p_{3/2}$  can explain a relatively strong  $B(M1)$  transition. The higher wave-function content of  $\nu p_{1/2}$  neutrons for the KB3G and GXPF1A interactions and the change in wave functions for the  $5/2^- \rightarrow 3/2^-$  ground-state transition can explain the relatively increased  $B(M1)$  value. However, in

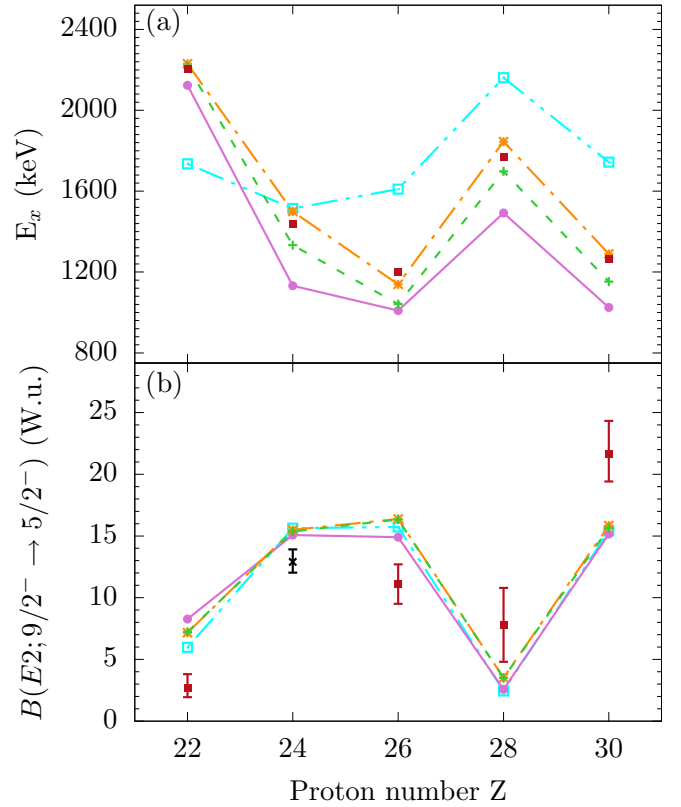


FIG. 5. (a) Calculated and experimental excitation energies  $E_x$  in keV for the  $9/2^-$  state and (b)  $B(E2, 9/2^- \rightarrow 5/2^-)$  values in W.u. (from Refs. [18,27–34] and this paper) for the isotones with  $N = 31$ . The shell-model interactions FPD6, KB3G, GXPF1A, and GXPF1Br were used. (The symbols and line styles as in Fig. 4 are used for values from different interactions and the experimental results.)

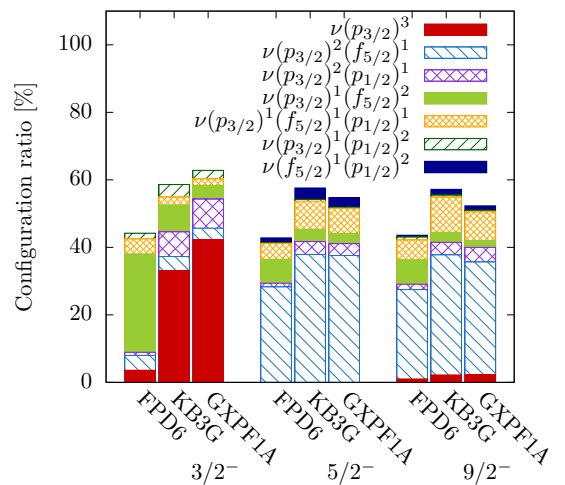


FIG. 6. The dominant neutron configurations of the  $3/2_{g.s.}^-$  ground state and the first  $5/2^-$ ,  $9/2^-$  states. The corresponding proton configuration is in all cases  $\pi(f_{7/2})^4$ . Configurations with contributions  $> 1\%$  for the interactions FPD6, KB3G, and GXPF1A are shown.

all cases the dominant transition  $\nu p_{3/2} \leftrightarrow \nu f_{5/2}$  explains the weak  $B(M1)$  strength from all interactions.

Another important aspect of the  $B(M1)$  transition probability is the particle-hole excitations for the neutrons and protons. In  $^{55}\text{Cr}$  the neutron core excitation can reproduce the relatively strong  $B(M1)$  strength because the neutron np-nh excitation corresponds to a spin-flip  $\nu f_{7/2} \leftrightarrow \nu f_{5/2}$ . Therefore, it can be speculated that all three shell-model interactions include a too weak neutron core excitation in  $^{55}\text{Cr}$ . The amount of proton spin-flip  $f_{7/2} \leftrightarrow f_{5/2}$  components could be neglected in comparison to the neutron as truncated shell-model results only show a marginal difference.

It is noteworthy to compare our findings with recent results obtained in the lighter  $Z = 22$  isotope  $^{53}\text{Ti}$  by Ref. [32]. In contrast to the measured  $B(M1; 5/2^- \rightarrow 3/2^-)$  value in  $^{55}\text{Cr}$  only an experimental upper limit was obtained for the same transition  $^{53}\text{Ti}$ . Although all shell-model interactions underestimated the experimental value of the  $B(M1; 5/2^- \rightarrow 3/2^-)$  value in  $^{55}\text{Cr}$ . In  $^{53}\text{Ti}$  the KB3G and GXPF1A interactions yielded higher  $B(M1; 5/2^- \rightarrow 3/2^-)$  values than the experimental limit, and the FPD6 interaction gave a small result consistent and below the upper limit. An analysis of the wave functions showed that for the first  $5/2^-$  state the FPD6 interaction is dominated by a  $\nu(f_{7/2})^8(p_{3/2})^2(f_{5/2})^1$  ( $\approx 55\%$ ) configuration with the protons coupled to spin zero. For the GXPF1A interaction the dominant configurations are the combination of  $\nu(f_{7/2})^8(p_{3/2})^3$  ( $\approx 36\%$ ) with the protons coupled to spin 2 and a  $\nu(f_{7/2})^8(p_{3/2})^2(p_{1/2})^1$  part ( $\approx 32\%$ ).

For  $^{53}\text{Ti}$  the calculations with the GXPF1A interaction yield that the np-nh neutron excitations across the  $N = 28$  shell work destructively on the  $M1$  strength of the  $5/2^- \rightarrow 3/2^-$  transition [32]. This is related to the reduced amount of the  $\nu(p_{3/2})^3$  configuration in the  $3/2^-_{\text{g.s.}}$  state and the contribution of the  $\nu(p_{3/2})^2(p_{1/2})^1$  configuration in the  $5/2^-_1$  state. These configurations cause a reduction of the  $M1$  strengths down to the values shown in Fig. 4(b). In case the neutron np-nh excitations would be increased even more, it is expected that the theoretical  $B(M1)$  value would approach the experimental value in  $^{53}\text{Ti}$ . Hence, an increase in neutron np-nh excitation across the  $N = 28$  shell gap would help to explain consistently the observed differences—a smaller  $M1$  transition strength in  $^{53}\text{Ti}$  and a slightly larger  $M1$  strength in  $^{55}\text{Cr}$ —between experiment and shell-model results. The new findings are also compared with the structure expected by a particle-plus-rotor model of low-lying states in  $^{55}\text{Cr}$ . The excited states are grouped into members of the  $K^\pi = 3/2^-$  ground-state band and a second excited  $K^\pi = 1/2^-$  band. The  $B(E2)$  strength of transitions are obtained by a shell-model calculation employing the GXPF1A interaction.  $B(E2)$  values larger than  $80 e^2\text{fm}^4$  are shown as black arrows in Fig. 7. Highest  $B(E2)$  values are given for transitions between the favored or the unfavored members of the two rotational structures. The new experimental result of a strong  $9/2^- \rightarrow 5/2^-$   $E2$  transition is corresponding to the  $E2$  transition within the favored part of the  $K^\pi = 1/2^-$  band; whereas the  $5/2^- \rightarrow 3/2^-$   $M1$  transition has to be considered as an intraband transition linking the excited  $K^\pi = 1/2^-$  band and the  $K^\pi = 3/2^-$  ground-state band. The missing  $E2$  strength

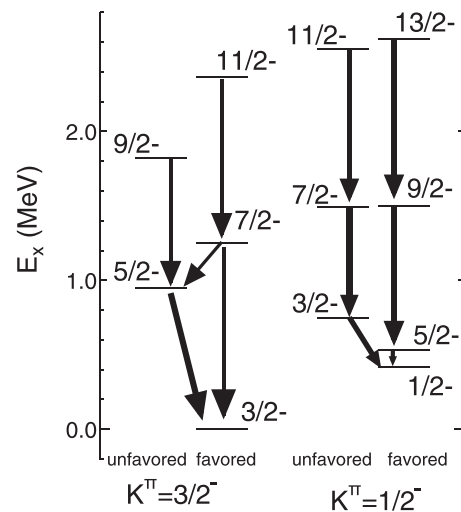


FIG. 7. The excitation energies and  $B(E2)$  strengths of the low-lying transitions in  $^{55}\text{Cr}$  are given obtained by the shell-model calculation using the GXPF1A interaction. The  $B(E2)$  values larger than  $80 e^2\text{fm}^4$  are shown as black arrows.

for this transition is explained by the different structure of the two rotational bands. Unfortunately, the experimental data did not allow to verify the reduced transition probability of other transitions.

## V. CONCLUSIONS

To summarize, precise lifetime values for the  $5/2^-$  and  $9/2^-$  states in  $^{55}\text{Cr}$  were determined improving rudimentary previous results. The experimentally deduced transition probabilities and the excitation energies were compared with shell-model calculations not only for  $^{55}\text{Cr}$ , but also along the  $N = 31$  chain of isotones from  $^{53}\text{Ti}$  to  $^{61}\text{Zn}$ . Different shell-model calculations employing the KSHELL code [19] as well as the code NUSHELLX@MSU [20] were performed in the  $fp$  model space consisting of the  $0f_{7/2}$ ,  $1p_{3/2}$ ,  $1p_{1/2}$ , and  $0f_{5/2}$  orbitals, coupled to a  $^{40}\text{Ca}$  inert core. The four interactions FPD6, GXPF1A, GXPF1Br, and KB3G [22] were compared with the experimental data.

The shell-model approaches using various interactions account for the global trend of  $E_x(9/2^-)$  energies and the  $B(E2; 9/2^- \rightarrow 5/2^-)$  values. The evidence for a remaining subshell closure in Cr isotopes at  $N = 32$  were confirmed. Discrepancies between experimental and theoretical  $B(M1; 5/2^- \rightarrow 3/2^-)$  values motivated a detailed analysis of the underlying wave function content of the  $3/2^-_{\text{g.s.}}$ ,  $5/2^-$ , and  $9/2^-$  states. The  $M1$  transition strength values of all four interactions are below the experimental results. The wave-function analysis shows that the reason for the difference is expected to be similar for the GXPF1A and KB3G interactions. However, the wave-function content of the  $3/2^-_{\text{g.s.}}$  ground state is distinctly different. It is concluded that an increase in neutron np-nh excitation across the  $N = 28$  shell gap would remedy the observed differences between experiment and shell model by increasing the  $M1$  strength in  $^{55}\text{Cr}$ . Simultaneously, an increased neutron np-nh excitation



would cause a smaller  $M1$  transition strength in the lighter isotone  $^{53}\text{Ti}$  and can resolve the discrepancy in  $M1$  strength also in this nucleus.

A consistent interpretation of the transition strength values in  $^{55}\text{Cr}$  is achieved within a shell-model based particle-plus-rotor model description. However, in this case a comprehensive comparison has to be based on an extended set of

measured lifetime values which will be the subject of future investigations.

#### ACKNOWLEDGMENTS

We thank the IKP FN tandem accelerator team for the support during the experiment.

- 
- [1] T. Otsuka, R. Fujimoto, Y. Utsuno, B. A. Brown, M. Honma, and T. Mizusaki, Magic Numbers in Exotic Nuclei and Spin-Isospin Properties of the NN Interaction, *Phys. Rev. Lett.* **87**, 082502 (2001).
- [2] T. Otsuka, Y. Utsuno, R. Fujimoto, B. A. Brown, M. Honma, and T. Mizusaki, Frontiers and challenges of the nuclear shell model, *Eur. Phys. J. A* **13**, 69 (2002).
- [3] H. Grawe, New vista of shell structure in neutron-rich exotic nuclei, *Acta Phys. Pol.*, B **34**, 2267 (2003).
- [4] H. Grawe, Shell model from a practitioner's point of view, in *The Euroschool Lectures on Physics with Exotic Beams* (Springer, Berlin, 2004), Vol. I, pp. 33–75.
- [5] T. Otsuka, T. Suzuki, R. Fujimoto, D. Abe, H. Grawe, and Y. Akaishi, Evolution of shell and collective structures in exotic nuclei, *Acta Phys. Pol.*, B **36**, 1213 (2005).
- [6] T. Otsuka, A. Gade, O. Sorlin, T. Suzuki, and Y. Utsuno, Evolution of shell structure in exotic nuclei, *Rev. Mod. Phys.* **92**, 015002 (2020).
- [7] D. Steppenbeck, S. Takeuchi, N. Aoi, P. Doornenbal, M. Matsushita, H. Wang, H. Baba, N. Fukuda, S. Go, M. Honma, J. Lee, K. Matsui, S. Michimasa, T. Motobayashi, D. Nishimura, T. Otsuka, H. Sakurai, Y. Shiga, P.-A. Söderström, T. Sumikama *et al.*, Evidence for a new nuclear 'magic number' from the level structure of  $^{54}\text{Ca}$ , *Nature (London)* **502**, 207 (2013).
- [8] T. Togashi, N. Shimizu, Y. Utsuno, T. Otsuka, and M. Honma, Large-scale shell-model calculations for unnatural-parity high-spin states in neutron-rich cr and fe isotopes, *Phys. Rev. C* **91**, 024320 (2015).
- [9] A. N. Deacon, D. Steppenbeck, S. Zhu, S. J. Freeman, R. V. F. Janssens, M. P. Carpenter, B. Fornal, M. Honma, B. P. Kay, F. G. Kondev, J. Kozemczak, A. Larabee, T. Lauritsen, C. J. Lister, A. P. Robinson, D. Seweryniak, J. F. Smith, Y. Sun, X. Wang, F. R. Xu *et al.*, Single-particle and collective structures in  $^{55}\text{Cr}$  and  $^{55}\text{V}$ , *Phys. Rev. C* **83**, 064305 (2011).
- [10] A. Bürger, T. R. Saito, H. Grawe, H. Hübel, P. Reiter, J. Gerl, M. Górski, H. J. Wollersheim, A. Al-Khatib, A. Banu, T. Beck, F. Becker, P. Bednarczyk, G. Benzoni, A. Bracco, S. Brambilla, P. Bringel, F. Camera, E. Clément, P. Doornenbal *et al.*, Relativistic Coulomb excitation of neutron-rich  $^{54,56,58}\text{Cr}$ : On the pathway of magicity from  $N = 40$  to  $N = 32$ , *Phys. Lett. B* **622**, 29 (2005).
- [11] M. Seidlitz, P. Reiter, A. Dewald, O. Möller, B. Bruyneel, S. Christen, F. Finke, C. Fransen, M. Górski, H. Grawe, A. Holler, G. Ilie, T. Kotthaus, P. Kudejová, S. M. Lenzi, S. Mandal, B. Melon, D. Mücher, J.-M. Regis, B. Saha *et al.*, Precision lifetime measurements of the first  $2^+$  and  $4^+$  states in  $^{56}\text{Cr}$  at the  $N=32$  subshell closure, *Phys. Rev. C* **84**, 034318 (2011).
- [12] D. E. Appelbe, C. J. Barton, M. H. Muikku, J. Simpson, D. D. Warner, C. W. Beausang, M. A. Caprio, J. R. Cooper, J. R. Novak, N. V. Zamfir, R. A. E. Austin, J. A. Cameron, C. Malcolmson, J. C. Waddington, and F. R. Xu, Detailed  $\gamma$ -ray spectroscopy of  $^{55}\text{Cr}$  and  $^{56}\text{Cr}$ : Confirmation of the subshell closure at  $N = 32$ , *Phys. Rev. C* **67**, 034309 (2003).
- [13] A. Dewald, S. Harissopulos, and P. von Brentano, The differential plunger and the differential decay curve method for the analysis of recoil distance Doppler-shift data, *Z. Phys. A: Atomic Nuclei* **334**, 163 (1989).
- [14] A. Dewald, O. Möller, and P. Petkov, Developing the Recoil Distance Doppler-Shift technique towards a versatile tool for lifetime measurements of excited nuclear states, *Prog. Part. Nucl. Phys.* **67**, 786 (2012).
- [15] K. Arnsward, T. Braunroth, M. Seidlitz, L. Coraggio, P. Reiter, B. Birkenbach, A. Blazhev, A. Dewald, C. Fransen, B. Fu, A. Gargano, H. Hess, R. Hirsch, N. Itaco, S. M. Lenzi, L. Lewandowski, J. Litzinger, C. Müller-Gatermann, M. Queiser, D. Rosiak *et al.*, Enhanced collectivity along the  $N = Z$  line: Lifetime measurements in  $^{44}\text{Ti}$ ,  $^{48}\text{Cr}$ , and  $^{52}\text{Fe}$ , *Phys. Lett. B* **772**, 599 (2017).
- [16] T. C. Braunroth, Lifetime measurements in neutron-rich isotopes close to  $N = 40$  and development of a simulation tool for RDDS spectra, Ph.D. thesis, Universität zu Köln, 2017.
- [17] G. Böhm, A. Dewald, P. Petkov, and P. von Brentano, The differential decay curve method for the analysis of doppler shift timing experiments, *Nucl. Instrum. Methods Phys. Res., Sect. A* **329**, 248 (1993).
- [18] A. M. Nathan, J. W. Olness, E. K. Warburton, and J. B. McGrory, Yrast decay schemes from heavy-ion+ $^{48}\text{Ca}$  fusion-evaporation reactions. III.  $^{57,58}\text{Fe}$ ,  $^{54,55}\text{Cr}$ , and  $^{57,58}\text{Mn}$ , *Phys. Rev. C* **17**, 1008 (1978).
- [19] N. Shimizu, T. Mizusaki, Y. Utsuno, and Y. Tsunoda, Thick-restart block Lanczos method for large-scale shell-model calculations, *Comput. Phys. Commun.* **244**, 372 (2019).
- [20] B. A. Brown and W. D. M. Rae, The shell-model code NuShellX@MSU, *Nucl. Data Sheets* **120**, 115 (2014).
- [21] W. A. Richter, M. G. van der Merwe, R. E. Hulies, and B. A. Brown, New effective interactions for the  $0f1_p$  shell, *Nucl. Phys. A* **523**, 325 (1991).
- [22] A. Poves, J. Sánchez-Solano, E. Caurier, and F. Nowacki, Shell model study of the isobaric chains  $A = 50$ ,  $A = 51$  and  $A = 52$ , *Nucl. Phys. A* **694**, 157 (2001).
- [23] M. Honma, T. Otsuka, B. A. Brown, and T. Mizusaki, Shell-model description of neutron-rich pf-shell nuclei with a new effective interaction GXPF1, *Eur. Phys. J. A* **25**, 499 (2005).
- [24] M. Honma, T. Otsuka, B. A. Brown, and T. Mizusaki, Effective interaction for pf-shell nuclei, *Phys. Rev. C* **65**, 061301 (2002).
- [25] T. Otsuka, M. Honma, and T. Mizusaki, Structure of the  $N = Z = 28$  Closed Shell Studied by Monte Carlo Shell Model Calculation, *Phys. Rev. Lett.* **81**, 1588 (1998).
- [26] M. Honma, T. Otsuka, B. A. Brown, and T. Mizusaki, New effective interaction for  $pf$ -shell nuclei and its implications for

- the stability of the  $N = Z = 28$  closed core, *Phys. Rev. C* **69**, 034335 (2004).
- [27] G. D. Sprouse and S. S. Hanna, Lifetimes and magnetic moments of levels in  $^{57}\text{Fe}$ , *Nucl. Phys. A* **137**, 658 (1969).
- [28] J. D. Hutton, N. R. Roberson, C. R. Gould, and D. R. Tilley, A study of low-lying levels in  $^{59}\text{Ni}$ , *Nucl. Phys. A* **206**, 403 (1973).
- [29] D. C. S. White, W. J. McDonald, D. A. Hutcheon, and G. C. Neilson, Pulsed beam lifetime measurements in  $^{64}\text{Cu}$ ,  $^{59}\text{Ni}$ ,  $^{65}\text{Zn}$ ,  $^{45,47,49}\text{Ti}$  and  $^{47,49,50,51}\text{V}$ , *Nucl. Phys. A* **260**, 189 (1976).
- [30] M. Queiser, A. Vogt, M. Seidlitz, P. Reiter, T. Togashi, N. Shimizu, Y. Utsuno, T. Otsuka, M. Honma, P. Petkov, K. Arnsward, R. Altenkirch, B. Birkenbach, A. Blazhev, T. Braunroth, A. Dewald, J. Eberth, C. Fransen, B. Fu, H. Hess *et al.*, Cross-shell excitations from the fp shell: Lifetime measurements in  $^{61}\text{Zn}$ , *Phys. Rev. C* **96**, 044313 (2017).
- [31] B. Fornal, S. Zhu, R. V. F. Janssens, M. Honma, R. Broda, B. A. Brown, M. P. Carpenter, S. J. Freeman, N. Hammond, F. G. Kondev, W. Królas, T. Lauritsen, S. N. Liddick, C. J. Lister, S. Lunardi, P. F. Mantica, N. Marginean, T. Mizusaki, E. F. Moore, T. Otsuka *et al.*, Yrast structure of neutron-rich  $^{53}\text{Ti}$ , *Phys. Rev. C* **72**, 044315 (2005).
- [32] A. Goldkuhle, A. Blazhev, C. Fransen, A. Dewald, M. Beckers, B. Birkenbach, T. Braunroth, E. Clément, J. Dudouet, J. Eberth, H. Hess, B. Jacquot, J. Jolie, Y.-H. Kim, A. Lemasson, S. M. Lenzi, H. J. Li, J. Litzinger, C. Michelagnoli, C. Müller-Gatermann *et al.*, Lifetime measurements of excited states in neutron-rich  $^{53}\text{Ti}$ : Benchmarking effective shell-model interactions, *Phys. Rev. C* **102**, 054334 (2020).
- [33] M. Pichevar, J. Delaunay, and B. Delaunay, Lifetime Measurements in  $^{59}\text{Ni}$  and  $^{57}\text{Ni}$ , *Nucl. Phys. A* **224**, 34 (1974).
- [34] V. K. Mittal, D. K. Avasthi, and I. M. Govil, Study of low-lying levels in  $^{59}\text{Ni}$ , *J. Phys. G: Nucl. Part. Phys.* **9**, 91 (1983).